IEEE Access
Multidisciplinary | Rapid Review | Open Access Journal

Received September 14, 2017, accepted October 8, 2017, date of publication October 11, 2017,
date of current version November 14, 2017.

Digital Object Identifier 10.1109/ACCESS.2017.2761889

Coordinated Control Strategies for SMES-Battery Hybrid Energy Storage Systems

XIAODONG LIN AND YONG LEI
School of Electrical Engineering and Information, Sichuan University, Chengdu, 610065, China
Corresponding author: Xiaodong Lin (605504139@qq.com)

ABSTRACT Power swings may cause power system instability; therefore, hybrid energy storage systems (HESSs) are necessary to smooth the output of wind farms. Superconducting magnetic energy storage (SMES) systems have a high power density, whereas battery energy storage systems (BESSs) provide a high energy density. The significant contribution of this paper is the proposal of hierarchical control strategies for an HESS composed of an SMES system and a BESS. Mathematical models and port-controlled Hamiltonian (PCH) models of the HESS are established. At the device level, a novel HESS control strategy based on the PCH models is proposed to improve its output performance. At the system level, a multilevel power allocation method based on empirical mode decomposition, Fuzzy control and advanced control is proposed to achieve an efficient grid connection for a wind farm; the grid connection considers the real-time and future state of charge of the SMES system and BESS. The effectiveness of the proposed strategies are verified through simulation studies.

INDEX TERMS BESS, coordinated control strategy, HESS, SMES.

I. INTRODUCTION

Energy storage systems (ESSs), which can achieve bidirectional power control, have attracted increasing interest in various fields for industrial applications due to their power and energy characteristics [1]. Common rechargeable batteries have a high energy density and long lifecycle, and they have been widely used in the power industry in standby power supplies and electric vehicles and for load following [2], [3]. However, such batteries have problems, such as their limited current rate, low response time, limited power density, and environmental hazards [4]. In addition, supercapacitors (SCs) and superconducting magnetic energy storage (SMES) systems are energy storage technologies with a high power density that are best suited for transient disturbance conditions [5]. For SCs, the accuracy of the model is critical because it is necessary to describe the charge-discharge processes using an equivalent model that involves complex nonlinear physical and chemical behaviors [6]–[8]. Moreover, the voltage of each cell in an SC is very low; hence, SCs should be connected in series when they are applied in electric vehicles or for new energy power generation. Thus, SCs incur problems because of their nonuniform cells, control complexity, and large range of terminal voltages [9], [10]. For SMESs, the research cost is higher than the cost of SCs. Compared to SCs, the advantages of SMESs are their extremely high efficiency, long cycle life, high power rating and low self-discharge rate. These advantages are conducive to reducing the operating costs of SMES [11]. Moreover, the common basic topologies of SMESs are voltage source converters (VSCs), and the voltage of the superconducting magnet can be maintained at a constant value. Although SMESs do not have obvious cost advantages to date, the cost of SMESs has been decreasing in recent years with the development of high-temperature superconducting technologies that enable the possibility of using SMESs as power systems on a large scale in the future [12], [13]. Considering that Li-ion batteries have been widely applied in large commercial energy management projects [14], hybrid energy storage systems (HESSs) composed of SMESs and Li-ion BESSs, which has both ideal power and energy characteristics, can be more effective than a single ESS.

Because of the use of power electronic devices, HESSs have multiple variables and exhibit nonlinearity and strong coupling during operation, and their control performance greatly impacts the system stability [15]. In order to ensure the reliability and robustness of HESSs, advanced control strategies are necessary. At present, the common linear control [16], [17] methods and nonlinear control methods [18]–[22] have not considered the internal or external interconnection structure of the system. The passivity-based

control (PBC) theory holds that a passive system will eventually run at the lowest energy point due to the dissipation caused by the structure of the system. For PBC using Euler-Lagrange models, only damping injection can be performed. For PBC using port-controlled Hamiltonian (PCH) models, both damping injection and energy shaping can be carried out [23]. Energy shaping (ES) is a control process used to stabilize a system at an expected equilibrium point by injecting external energy into the controlled system. Romeo Ortega and Arjan van der Schaft first proposed the interconnection and damping assignment passivity-based control (IDA-PBC) method based on PCH models [24]–[27]. This method considers the interconnection structure of the system [24] and avoids introducing the Casimir function. Low control complexity is a significant advantage of the IDA-PBC method; therefore, it can conveniently provide ES. ES control has been widely used in robotics [28], PWM rectifiers [29], double-fed wind power systems [30]–[32], and battery energy storage systems (BESSs) [33]. Since the HESS cannot generate energy independently, it is a typical passive system. The laws of the energy flow of an HESS can be revealed by studying its interconnection structure. By considering both the nonlinear nature of a system and the energy flow, ES control can achieve better control performance than conventional control strategies for HESSs. There is currently a lack of research on using the ES control strategy for HESSs; therefore, applying ES control to HESSs based on PCH models has practical significance.

In order to achieve the efficient, safe and stable operation of an HESS, a reasonable power allocation strategy is crucial. The common power allocation strategies include inertia filters [34]–[39], Fourier transforms [40], and wavelet decomposition [41], [42]. Reference [34] and [35] used low-pass filters for power allocation, but they did not consider the SOC limitations; ESSs are prone to overcharging and overdischarging. Based on this behavior, Shao *et al.* [36] introduced small amplitude fluctuations that provided a certain regulatory space for the SOC of a BESS. References [37]–[39] combined the filter and the SOC together, and the filter time constant is the central component of this kind of allocation strategy. The research in [37] established the objective function of the SOC and used a genetic algorithm to determine the cut-off frequency. Reference [38] used the moving average method, and the time constant was dynamically adjusted depending on the work status of the SOC. A double fuzzy logic control strategy for optimizing the SOC was proposed in [39], and the time constant of the low-pass filter was adjusted by using fuzzy rules. Although the methods in [37]–[39] can effectively smooth the wind power fluctuations and avoid overcharging or deep discharging, they cannot ensure that the SOC will be maintained at a relatively high state during operation. Additionally, both the inertia filter method and moving average method have a certain time lag that causes waveform distortion in some cases and affects the effectiveness of the power compensation [40]. In addition, it is also difficult to reliably determine the most important time constant [41]–[43]. The conclusions from [44] indicate that the time constant of the filter needs to be weighed against factors such as the device lifetime, capacity, and power characteristics, and currently, the quantitative correlations cannot be accurately described. To solve these problems, [45] and [46] used spectral analyses based on Fourier transforms to determine the compensation frequency band of ESSs. But Fourier transforms have significant limitations when analyzing nonstationary signals, and they cannot make full use of the essential characteristics of signals. Han *et al.* [47] adopted wavelet theory to realize the multilayer decomposition of the power output of wind power; their method effectively overcame the time lags caused by the inertia filter method. However, further research on the optimization of the SOC has not been conducted. The wavelet decomposition has an unsatisfactory time-frequency resolution, and it is difficult to obtain detailed information regarding the high-frequency part of the signal [48].

This significant study focuses on coordinated control strategies for HESSs. Considering the internal or external interconnection structure of the system, ES control based on PCH models is proposed at the device level to achieve better output characteristics for the HESS. In order to achieve reasonable power allocation, effectively optimize the SOC and make full use of the essential characteristics of the signals, a novel system-level control strategy is proposed. Empirical mode decomposition (EMD), which is an ideal tool for nonstationary signal analysis, is adopted for the initial power allocation to overcome the time lags of the conventional methods. Considering the real-time and future SOC levels, a fuzzy control and an advanced control strategy are designed for secondary allocation; these methods allow the HESS to effectively stabilize the power fluctuations caused by wind farms and maintain the SOC within a relatively high state during operation.

The remainder of this paper is arranged as follows. The mathematical models, PCH models of the HESS, and the detail hierarchical control strategies of HESS are described in Section II. The simulation results are discussed in Section III, and the key conclusions are summarized in Section IV.

II. COORDINATED CONTROL STRATEGIES FOR HESSs

A. MATHEMATIC MODELS OF HESS

The topological structure of the HESS is shown in Fig. 1. The SMES and BESS are connected to the AC side of the converter. There are two types of conventional converters: VSCs and current source converters. A VSC can maintain the stability of the DC-side voltage and is thus selected as the basic circuit here.

Each phase bridge arm of the VSC contains two switching tubes. The status of the switching tubes can be expressed as $S_k, k = a, b, c/A, B, C$. The switch state can be expressed as

$$S_k = \begin{cases} 1, & S_{k1} = 1, \quad S_{k2} = 0 \\ 0, & S_{k1} = 0, \quad S_{k2} = 1 \end{cases} \tag{1}$$

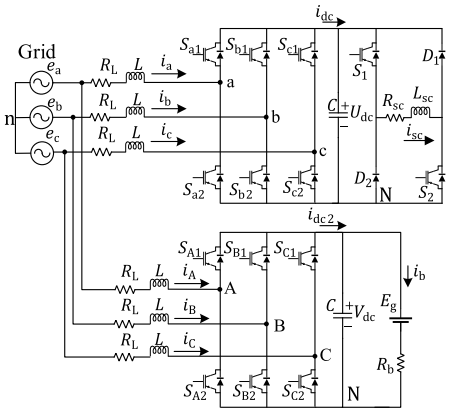

FIGURE 1. Topological structure of the HESS.

Then, U_{Nn} and U_{Mn} can be respectively represented as

$$\begin{cases} U_{\mathrm{Nn}} = -\frac{1}{3}U_{\mathrm{dc}} \sum\limits_{k=\mathrm{a,b,c}} (S_k - 1) \\ U_{\mathrm{Mn}} = -\frac{1}{3}V_{\mathrm{dc}} \sum\limits_{k=\mathrm{A,B,C}} (S_k - 1) \end{cases} \tag{2}$$

By applying Kirchhoff's law, the mathematical model of the converter of the SMES in dq coordinates can be expressed as

$$\begin{cases} L(di_{\mathrm{d}})/dt = -R_{\mathrm{L}}i_{\mathrm{d}} + \omega L i_{\mathrm{q}} - S_{\mathrm{d}}U_{\mathrm{dc}} + V_{\mathrm{gd}} \\ L(di_{\mathrm{q}})/dt = -\omega L i_{\mathrm{d}} - R_{\mathrm{L}}i_{\mathrm{q}} - S_{\mathrm{q}}U_{\mathrm{dc}} + V_{\mathrm{gq}} \end{cases} \tag{3}$$

where R_{L} and L represent the value of AC-side resistance and inductor, respectively; i_{d} and i_{q} represent the direct and quadrature axis currents of the SMES, respectively; V_{gd} and V_{gq} represent the direct and quadrature axis grid side voltages, respectively; ω represents the angular frequency of the grid side voltage; U_{dc} is the voltage of DC-side capacitor of the SMES; and S_{d} and S_{q} represent the direct and quadrature axis switching functions of the SMES, respectively.

The chopper of the SMES system has three operating modes: (1) charging state; (2) freewheeling state; and (3) discharging state. Here, d_1 and d_2 are the duty cycles of the corresponding insulated gate bipolar transistor (IGBT), S_1 and S_2 in the chopper, respectively. Assuming that the duty cycle $d_1 = d_2 = D$, the mathematical model of the DC-side chopper can be expressed as

$$\begin{cases} L\mathrm{sc}(di_{\mathrm{sc}})/dt = -R\mathrm{sc}i\mathrm{sc} + (2D-1)\,U_{\mathrm{dc}} \\ C(dU_{\mathrm{dc}})/dt = i_{\mathrm{dc}} - (2D-1)\,i_{\mathrm{sc}} \end{cases} \tag{4}$$

where R_{sc} and L_{sc} represent the value of the resistance and inductor of the magnet; C represents the value of DC-side capacitor; and D represents the duty cycle of S_1 and S_2.

If the duty cycle D is less than 0.5, then the magnet releases energy into the power grid; if the duty cycle D is greater than 0.5, then the magnet absorbs energy from the power grid.

Similarly, the mathematical model of the converter of the BESS in dq coordinates can be expressed as

$$\begin{cases} L(di_{\mathrm{D}})/dt = -R_{\mathrm{L}}i_{\mathrm{D}} + \omega L i_{\mathrm{Q}} - S_{\mathrm{D}}V_{\mathrm{dc}} + V_{\mathrm{gd}} \\ L(di_{\mathrm{Q}})/dt = -\omega L i_{\mathrm{D}} - R_{\mathrm{L}}i_{\mathrm{Q}} - S_{\mathrm{Q}}V_{\mathrm{dc}} + V_{\mathrm{gq}} \\ \frac{2}{3}C\frac{dV_{\mathrm{dc}}}{dt} = S_{\mathrm{D}}i_{\mathrm{D}} + S_{\mathrm{Q}}i_{\mathrm{Q}} - \frac{2V_{\mathrm{dc}}}{3R_{\mathrm{b}}} + \frac{2E_{\mathrm{g}}}{3R_{\mathrm{b}}} \end{cases} \tag{5}$$

where i_{D} and i_{Q} represent the direct and quadrature axis currents of the BESS, respectively; E_{g} is the terminal voltage of the battery; R_{b} is the value of the internal resistance of the battery; V_{dc} is the voltage of DC-side capacitor of the BESS; and S_{D} and S_{Q} represent the direct and quadrature axis switching functions of the BESS, respectively.

B. PCH MODELS OF HESS

The specific design process of ES control includes three steps: constructing the PCH model, setting the desired equilibrium and solving the energy matching equation. Therefore, establishing the PCH model based on a mathematical model is very important and is the basis of the following design.

Because an HESS can only store and release energy and does not have the ability to generate electricity independently, it can be regarded as a typical passive system that meets the requirements of PCH modeling and ES control.

Considering the energy dissipation in the system, the general PCH model [23] can be written as

$$\begin{cases} \dot{\boldsymbol{x}} = [\boldsymbol{J}(\boldsymbol{x}) - \boldsymbol{R}(\boldsymbol{x})]\frac{\partial H(\boldsymbol{x})}{\partial \boldsymbol{x}} + \boldsymbol{g}(\boldsymbol{x})\boldsymbol{u} \\ \boldsymbol{y} = \boldsymbol{g}^{\mathrm{T}}(\boldsymbol{x})\frac{\partial H(\boldsymbol{x})}{\partial \boldsymbol{x}} \end{cases} \tag{6}$$

where $\boldsymbol{J}(\boldsymbol{x})$ is the internal structure matrix, which reflects the internal energy conversion structure; $\boldsymbol{R}(\boldsymbol{x})$ is the damping matrix, which reflects the energy dissipation characteristics of the system; $H(\boldsymbol{x})$ is the energy function of the system; $\boldsymbol{g}(\boldsymbol{x})$ is the internal and external interaction matrix, which reflects the internal and external energy transfer structure; $\boldsymbol{x}$ is the state vector; $\boldsymbol{u}$ is the input vector; $\boldsymbol{y}$ is the output vector; and the product of $\boldsymbol{u}$ and $\boldsymbol{y}$ represents the value of the power transmitted between the system and external systems. In addition, $\boldsymbol{J}(\boldsymbol{x})$ is anti-symmetric, and $\boldsymbol{R}(\boldsymbol{x})$ is symmetric positive semi-definite.

1) PCH MODEL FOR THE SMES

First, the energy function of the AC-side VSC of the SMES system is established as

$$H = \frac{1}{2}Li_{\mathrm{d}}^2 + \frac{1}{2}Li_{\mathrm{q}}^2 \tag{7}$$

The state vector of the VSC of the SMES is defined as

$$\boldsymbol{x} = [Li_{\mathrm{d}}\ Li_{\mathrm{q}}]^{\mathrm{T}} \tag{8}$$

With the same form as that of (6), the PCH model of the converter of the SMES can be obtained using (3), which can

be expressed as

$$\begin{pmatrix} L\frac{di_d}{dt} \\ L\frac{di_q}{dt} \end{pmatrix} = \begin{pmatrix} -R_L & \omega L \\ -\omega L & -R_L \end{pmatrix} \begin{pmatrix} i_d \\ i_q \end{pmatrix} + \begin{pmatrix} -S_d \\ -S_q \end{pmatrix} U_{dc} + \begin{pmatrix} V_{gd} \\ V_{gq} \end{pmatrix} \tag{9}$$

where $\nabla H = \partial H(\boldsymbol{x})/\partial \boldsymbol{x} = [\, i_d \;\; i_q \,]^T$; the internal and external interaction matrices are $\boldsymbol{g}_1 = [-S_d \; -S_q)]^T$, $\boldsymbol{g}_2 = [\, 1 \;\; 0 \,]^T$, and $\boldsymbol{g}_3 = [\, 0 \;\; 1 \,]^T$; the input vectors are $\boldsymbol{u}_1 = U_{dc}$, $\boldsymbol{u}_2 = V_{gd}$, and $\boldsymbol{u}_3 = V_{gq}$; the output vectors are $\boldsymbol{y}_1 = \boldsymbol{g}_1^T \nabla H = -(S_d i_d + S_q i_q) = -i_{dc}$, $\boldsymbol{y}_2 = \boldsymbol{g}_2^T \nabla H = i_d$, and $\boldsymbol{y}_3 = \boldsymbol{g}_3^T \nabla H = i_q$; the internal structure matrix is $\boldsymbol{J} = \begin{pmatrix} 0 & \omega L \\ -\omega L & 0 \end{pmatrix}$; and the damping matrix is $\boldsymbol{R} = diag\,\{R_L\}$.

The internal and external interconnection matrix $\boldsymbol{g}(\boldsymbol{x})$ contains the switch functions S_d and S_q because the energy interaction between the system and power grid depends on the status of the IGBT tubes.

Second, the energy function of the DC-side chopper of the SMES system is established as

$$H = \frac{1}{2} C U_{dc}^2 + \frac{1}{2} L_{sc} i_{sc}^2 \tag{10}$$

The state vector of the chopper is defined as

$$\boldsymbol{x} = [\, C U_{dc} \;\; L_{sc} i_{sc} \,]^T \tag{11}$$

Assuming that the magnet resistance is $R_{sc} = 0$, in the corresponding form of (6), the PCH model of the converter can be obtained by (4), which is expressed as

$$\begin{pmatrix} C\frac{dU_{dc}}{dt} \\ L_{sc}\frac{di_{sc}}{dt} \end{pmatrix} = \begin{pmatrix} 0 & -(2D-1) \\ 2D-1 & 0 \end{pmatrix} \begin{pmatrix} U_{dc} \\ i_{sc} \end{pmatrix} + \begin{pmatrix} 1 \\ 0 \end{pmatrix} i_{dc} \tag{12}$$

where $\nabla H = \partial H(\boldsymbol{x})/\partial \boldsymbol{x} = [\, U_{dc} \quad i_{sc} \,]^T$; the interaction matrix is $\boldsymbol{g} = [\, 1 \quad 0 \,]^T$; the input vector is $\boldsymbol{u}_{21} = i_{dc}$; the output vector is $\boldsymbol{y}_{21} = \boldsymbol{g}^T \nabla H = U_{dc}$; the internal structure matrix is $\boldsymbol{J} = \begin{pmatrix} 0 & -(2D-1) \\ 2D-1 & 0 \end{pmatrix}$; and the damping matrix is $\boldsymbol{R} = (0)_{2\times 2}$.

Because $\mathbf{u}_1 = \mathbf{y}_{21} = U_{dc}$ and $\mathbf{y}_1 = -\mathbf{u}_{21} = -i_{dc}$, the AC-side VSC and DC-side chopper are cascaded via a feedback interconnection. The feedback interconnection structure remains unchanged in the PCH models of the cascaded systems and fully embodies the energy transfer process between the AC-side VSC and DC-side chopper; thus, this structure provides a means for controlling the energy flow of the controlled system. The feedback interconnection structure of the controlled SMES system is shown in Fig. 2.

2) PCH MODEL FOR THE BESS

The energy function of the BESS is established as

$$H = \frac{1}{2} L i_D^2 + \frac{1}{2} L i_Q^2 + \frac{1}{2} C V_{dc}^2 \tag{13}$$

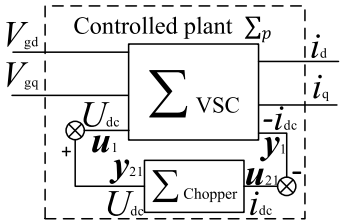

FIGURE 2. Feedback interconnection structure of the SMES system.

The state vector of the BESS is defined as

$$\boldsymbol{x} = [\, L i_D \quad L i_Q \quad C V_{dc} \,]^T \tag{14}$$

With the same form as that of (6), the PCH model of the converter of the BESS can be obtained using (5), which can be expressed as

$$\begin{pmatrix} L\frac{di_D}{dt} \\ L\frac{di_Q}{dt} \\ \frac{2}{3}C\frac{dV_{dc}}{dt} \end{pmatrix} = \begin{pmatrix} -R_L & \omega L & -S_D \\ -\omega L & -R_L & -S_Q \\ S_D & S_Q & -\frac{2}{3R_b} \end{pmatrix} \begin{pmatrix} i_D \\ i_Q \\ V_{dc} \end{pmatrix} + \begin{pmatrix} V_{gd} \\ V_{gq} \\ \frac{2E_g}{3R_b} \end{pmatrix} \tag{15}$$

where $\nabla H = \partial H(\boldsymbol{x})/\partial \boldsymbol{x} = \left[\, i_D \; i_Q \; V_{dc} \,\right]^T$; the internal and external interaction matrices are $\boldsymbol{g}_1 = [\, 1 \; 0 \; 0 \,]^T$, $\boldsymbol{g}_2 = [\, 0 \; 1 \; 0 \,]^T$, and $\boldsymbol{g}_3 = [\, 0 \; 0 \; 1 \,]^T$; the input vectors are $\boldsymbol{u}_1 = V_{gd}$, $\boldsymbol{u}_2 = V_{gq}$, and $\boldsymbol{u}_3 = 2E_g/(3R_b)$; the output vectors are $\boldsymbol{y}_1 = \boldsymbol{g}_1^T \nabla H = i_D$, $\boldsymbol{y}_2 = \boldsymbol{g}_2^T \nabla H = i_Q$, and $\boldsymbol{y}_3 = \boldsymbol{g}_3^T \nabla H = V_{dc}$; the internal structure matrix is

$$\boldsymbol{J} = \begin{bmatrix} 0 & \omega L & -S_D \\ -\omega L & 0 & -S_Q \\ S_D & S_Q & 0 \end{bmatrix};$$

and the damping matrix is

$$\boldsymbol{R} = \begin{bmatrix} R_L & 0 & 0 \\ 0 & R_L & 0 \\ 0 & 0 & -2/(3R_b) \end{bmatrix}.$$

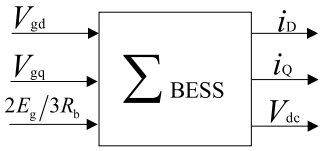

FIGURE 3. PCH structure of the BESS.

The switch functions S_D and S_Q are contained in the internal structure matrix $\boldsymbol{J}(\boldsymbol{x})$, which explains that the energy transfer structure in the battery changes according to the switching function. The PCH structure of the BESS is shown in Fig. 3.

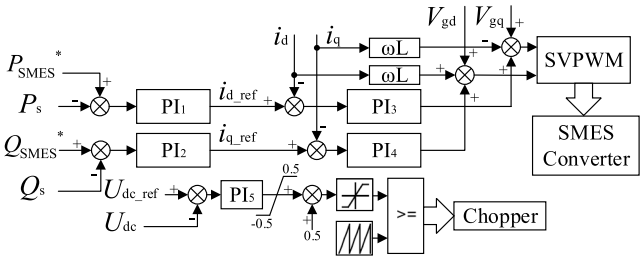

FIGURE 4. Traditional power control structure of the SMES system.

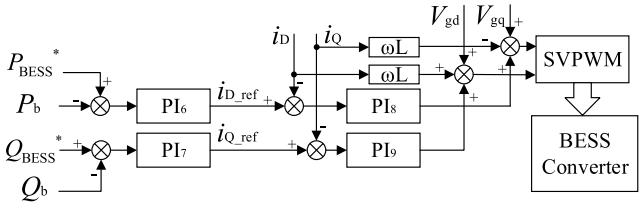

FIGURE 5. Traditional power control structure of the BESS.

C. DEVICE-LEVEL CONTROL STRATEGY

The structures of the traditional power control of an HESS are shown in Fig. 4 and Fig. 5. The active and reactive current references are obtained from the outer power loop control (PI_1 and PI_2/ PI_6 and PI_7), and the voltage commands required by the space vector pulse-width modulation (SVPWM) are obtained from the inner current loop control (PI_3 and PI_4 / PI_8 and PI_9) and the decoupling control. In particular, the voltage regulator (PI_5) controls the DC-side voltage of the converter of the SMES [16], [49]. The traditional control structure includes numerous PI controllers, and the parameters of the PI controllers must be modified repeatedly. However, it is difficult to achieve the desired effect and provide a clear physical implication using so many PI controllers. Therefore, ES control for the HESS is proposed in this section; this control considers both the nonlinear nature of a system and the energy flow.

1) PROPOSED ES CONTROL FOR THE SMES

Because the SMES system is cascaded via feedback interconnection, it is necessary to reduce the system dimensions to solve the control variables. It is very difficult to establish the Casimir function, which is the traditional method used to reduce the system dimensions. Therefore, this study first uses the feedback interconnection method for cascading between the subsystems and then establishes the energy matching equation using the energy-based control method [30] to determine the control variables.

The dynamic equations of the system can be expressed as

$$\dot{\boldsymbol{x}} = [\boldsymbol{J}(\boldsymbol{x}) - \boldsymbol{R}(\boldsymbol{x})]\frac{\partial H(\boldsymbol{x})}{\partial \boldsymbol{x}} + \boldsymbol{g}(\boldsymbol{x})\boldsymbol{u} \tag{16}$$

When the control energy is injected into the controlled system, the desired dynamic equations of the system can be expressed as

$$\dot{\boldsymbol{x}} = [\boldsymbol{J}_{\mathrm{d}}(\boldsymbol{x}) - \boldsymbol{R}_{\mathrm{d}}(\boldsymbol{x})]\frac{\partial H_{\mathrm{d}}(\boldsymbol{x})}{\partial \boldsymbol{x}} \tag{17}$$

with

$$\begin{cases} \boldsymbol{J}_{\mathrm{d}}(\boldsymbol{x}) = \boldsymbol{J}(\boldsymbol{x}) + \boldsymbol{J}_{\alpha}(\boldsymbol{x}) \\ \boldsymbol{R}_{\mathrm{d}}(\boldsymbol{x}) = \boldsymbol{R}(\boldsymbol{x}) + \boldsymbol{R}_{\alpha}(\boldsymbol{x}) \\ H_{\mathrm{d}}(\boldsymbol{x}) = H(\boldsymbol{x}) + H_{\alpha}(\boldsymbol{x}) \end{cases}$$

where $\boldsymbol{J}_{\mathrm{d}}(\boldsymbol{x})$, $\boldsymbol{R}_{\mathrm{d}}(\boldsymbol{x})$ and $H_{\mathrm{d}}(\boldsymbol{x})$ represent the desired internal structure matrix, the desired dissipation matrix and the expected energy function of the system, respectively; $\boldsymbol{J}_{\alpha}(\boldsymbol{x})$ and $\boldsymbol{R}_{\alpha}(\boldsymbol{x})$ represent the new generated internal structure and dissipative structure of the system, respectively; and $H_{\alpha}(\boldsymbol{x})$ represents the injected energy of the controller.

The main concept of ES control is that the controlled system will become stable at the desired energy function $H_{\mathrm{d}}(\boldsymbol{x})$. The control is established through the matrix $\boldsymbol{J}_{\alpha}(\boldsymbol{x})$. Then, the matrix $\boldsymbol{R}_{\alpha}(\boldsymbol{x})$ introduces the control energy $H_{\alpha}(\boldsymbol{x})$ to shape the desired energy $H_{\mathrm{d}}(\boldsymbol{x})$, forcing the system to operate around the desired non-zero equilibrium point; this process is why this method is called ES control.

The system control variable $\boldsymbol{u}$ can be solved using the energy matching equation

$$[\boldsymbol{J}(\boldsymbol{x}) - \boldsymbol{R}(\boldsymbol{x})]\frac{\partial H(\boldsymbol{x})}{\partial \boldsymbol{x}} + \boldsymbol{g}(\boldsymbol{x})\boldsymbol{u} = [\boldsymbol{J}_{\mathrm{d}}(\boldsymbol{x}) - \boldsymbol{R}_{\mathrm{d}}(\boldsymbol{x})]\frac{\partial H_{\mathrm{d}}(\boldsymbol{x})}{\partial \boldsymbol{x}} \tag{18}$$

The energy function of the VSC of the SMES system is represented as

$$H(\boldsymbol{x}) = \frac{1}{2}Li_{\mathrm{d}}^2 + \frac{1}{2}Li_{\mathrm{q}}^2 \tag{19}$$

The control objective of the AC-side converter is to make the converter track the power instruction effectively. The expected energy function of the VSC is expressed as

$$H_{\mathrm{d}}(\boldsymbol{x}) = \frac{1}{2}L(i_{\mathrm{d}} - i_{\mathrm{d}}^*)^2 + \frac{1}{2}L(i_{\mathrm{q}} - i_{\mathrm{q}}^*)^2 \tag{20}$$

The state variable at the equilibrium point of the AC-side converter is $\boldsymbol{x}^* = [Li_{\mathrm{d}}^* \; Li_{\mathrm{q}}^*]^{\mathrm{T}}$ therefore, if the converter operates around the desired equilibrium point, then $H_{\mathrm{d}}(\boldsymbol{x})$ should have a minimum value at the expected equilibrium point of the system, that is, $\dot{\boldsymbol{x}}|_{(\boldsymbol{x}=\boldsymbol{x}^*)} = 0$.

The equations for the active power and reactive power at the desired equilibrium point are written as

$$\begin{cases} P_{\mathrm{SMES}}^* = 3(V_{\mathrm{gd}}i_{\mathrm{d}}^* + V_{\mathrm{gq}}i_{\mathrm{q}}^*)/2 \\ Q_{\mathrm{SMES}}^* = 3(V_{\mathrm{gq}}i_{\mathrm{d}}^* - V_{\mathrm{gd}}i_{\mathrm{q}}^*)/2 \end{cases} \tag{21}$$

Then, the equilibrium points of the active and reactive currents can be calculated as

$$\begin{cases} i_{\mathrm{d}}^* = \dfrac{2(P_{\mathrm{SMES}}^* V_{\mathrm{gd}} + Q_{\mathrm{SMES}}^* V_{\mathrm{gq}})}{3\left(V_{\mathrm{gd}}^2 + V_{\mathrm{gq}}^2\right)} \\ i_{\mathrm{q}}^* = \dfrac{2(P_{\mathrm{SMES}}^* V_{\mathrm{gq}} - Q_{\mathrm{SMES}}^* V_{\mathrm{gd}})}{3\left(V_{\mathrm{gd}}^2 + V_{\mathrm{gq}}^2\right)} \end{cases} \tag{22}$$

Because $\dot{\boldsymbol{x}}|_{(\boldsymbol{x}=\boldsymbol{x}^*)}=0$, (9) should satisfy

$$\begin{pmatrix} -R_{\mathrm{L}} & \omega L \\ -\omega L & -R_{\mathrm{L}} \end{pmatrix}\begin{pmatrix} i_{\mathrm{d}}^* \\ i_{\mathrm{q}}^* \end{pmatrix}+\begin{pmatrix} -S_{\mathrm{d}} \\ -S_{\mathrm{q}} \end{pmatrix}U_{\mathrm{dc}}^*+\begin{pmatrix} V_{\mathrm{gd}} \\ V_{\mathrm{gq}} \end{pmatrix}=0 \tag{23}$$

where U_{dc}^* is the desired value of the DC-side voltage.

The equilibrium points of the switching functions can be calculated as

$$\begin{cases} S_{\mathrm{d}}^*=\dfrac{-R_{\mathrm{L}}i_{\mathrm{d}}^*+\omega L i_{\mathrm{q}}^*+V_{\mathrm{gd}}}{U_{\mathrm{dc}}^*} \\ S_{\mathrm{q}}^*=\dfrac{-R_{\mathrm{L}}i_{\mathrm{q}}^*-\omega L i_{\mathrm{d}}^*+V_{\mathrm{gq}}}{U_{\mathrm{dc}}^*} \end{cases} \tag{24}$$

We construct the matrices $\boldsymbol{J}_\alpha$ and $\boldsymbol{R}_\alpha$ as follows:

$$\boldsymbol{J}_\alpha=\begin{pmatrix} 0 & \omega L \\ -\omega L & 0 \end{pmatrix},\quad \boldsymbol{R}_\alpha=\mathrm{diag}\{R_1,R_2\}$$

where R_1 and R_2 are positive numbers used to vary the damping of the system, and we set $R_1=R_2=1\Omega$.

By solving the energy matching equation (18), the control law of the VSC of the SMES system can be solved as

$$\begin{cases} S_{\mathrm{d}}=S_{\mathrm{d}}^*+\dfrac{R_1\left(i_{\mathrm{d}}-i_{\mathrm{d}}^*\right)+\omega L\left(i_{\mathrm{q}}-i_{\mathrm{q}}^*\right)}{U_{\mathrm{dc}}^*} \\ S_{\mathrm{q}}=S_{\mathrm{q}}^*+\dfrac{R_2\left(i_{\mathrm{q}}-i_{\mathrm{q}}^*\right)-\omega L\left(i_{\mathrm{d}}-i_{\mathrm{d}}^*\right)}{U_{\mathrm{dc}}^*} \end{cases} \tag{25}$$

The energy function of the SMES chopper is represented as

$$H(\boldsymbol{x})=\frac{1}{2}CU_{\mathrm{dc}}^2+\frac{1}{2}L_{\mathrm{sc}}i_{\mathrm{sc}}^2 \tag{26}$$

The control objective of the chopper is to maintain the stability of the DC voltage and to achieve effective energy transmission between the AC and DC sides. The expected energy function of the chopper is expressed as

$$H_{\mathrm{d}}(\boldsymbol{x})=\frac{1}{2}L_{\mathrm{sc}}\left(i_{\mathrm{sc}}-i_{\mathrm{sc}}^*\right)^2+\frac{1}{2}C(U_{\mathrm{dc}}-U_{\mathrm{dc}}^*)^2 \tag{27}$$

where i_{sc}^* is the current command of the magnet, which is an intermediate variable that can be eliminated.

The state variable at the equilibrium point of the DC-side chopper is $\boldsymbol{x}^*=[\,CU_{\mathrm{dc}}^* \quad L_{\mathrm{sc}}i_{\mathrm{sc}}^*\,]^{\mathrm{T}}$; therefore, if the chopper operates around the equilibrium point, then $H_{\mathrm{d}}(\boldsymbol{x})$ should reach a minimum value at the expected equilibrium point of the system, that is, $\dot{\boldsymbol{x}}|_{(\boldsymbol{x}=\boldsymbol{x}^*)}=0$.

Because $\dot{\boldsymbol{x}}|_{(\boldsymbol{x}=\boldsymbol{x}^*)}=0$, (12) should satisfy

$$\begin{pmatrix} 0 & -(2D-1) \\ 2D-1 & 0 \end{pmatrix}\begin{pmatrix} U_{\mathrm{dc}}^* \\ i_{\mathrm{sc}}^* \end{pmatrix}+\begin{pmatrix} 1 \\ 0 \end{pmatrix}i_{\mathrm{dc}}=0 \tag{28}$$

The chopper balance point is $D=0.5$ for the SMES system to remain in the freewheeling state without control.

We construct the matrices $\boldsymbol{J}_\alpha$ and $\boldsymbol{R}_\alpha$ as follows:

$$\boldsymbol{J}_\alpha=(0)_{2\times 2},\quad \boldsymbol{R}_\alpha=\mathrm{diag}\{r_1,r_2\}$$

where r_1 and r_2 are positive numbers used to vary the damping of the chopper, and we set $r_1=r_2=0.1\Omega$.

We set the control variable $\boldsymbol{u}=D$, and we assume that $\nabla H_\alpha=\partial H_\alpha/\partial\mathbf{x}=\begin{bmatrix} k_1 & k_2 \end{bmatrix}^{\mathrm{T}}$ and the intermediate control variable $m=2D-1$. The energy matching equation of the chopper is then expressed as

$$\begin{pmatrix} -r_1 & -(2D-1) \\ 2D-1 & -r_2 \end{pmatrix}\begin{pmatrix} -U_{\mathrm{dc}}^* \\ -i_{\mathrm{sc}}^* \end{pmatrix}=\begin{pmatrix} r_1 & 0 \\ 0 & r_2 \end{pmatrix}\begin{pmatrix} U_{\mathrm{dc}} \\ i_{\mathrm{sc}} \end{pmatrix}+\begin{pmatrix} 1 \\ 0 \end{pmatrix}i_{\mathrm{dc}} \tag{29}$$

By solving the energy matching equation (18), the control law of the SMES chopper can be solved as (30), as shown at the bottom of this page. The actual control variable D can be obtained by $(m+1)/2$.

2) PROPOSED ES CONTROL FOR THE BESS

The energy function of the VSC of the BESS is represented as

$$H(\boldsymbol{x})=0.5Li_{\mathrm{D}}^2+0.5Li_{\mathrm{Q}}^2+0.5CV_{\mathrm{dc}}^2 \tag{31}$$

The control objective of the converter is to make the converter track the power instruction effectively and maintain the stability of the DC voltage.

The expected energy function of the VSC of the BESS is expressed as

$$H_{\mathrm{d}}(\boldsymbol{x})=\frac{1}{2}L(i_{\mathrm{D}}-i_{\mathrm{D}}^*)^2+\frac{1}{2}L(i_{\mathrm{Q}}-i_{\mathrm{Q}}^*)^2+\frac{1}{2}C(V_{\mathrm{dc}}-V_{\mathrm{dc}}^*)^2 \tag{32}$$

Because $\dot{\boldsymbol{x}}|_{(\boldsymbol{x}=\boldsymbol{x}^*)}=0$, (15) should satisfy

$$\begin{pmatrix} -R_{\mathrm{L}} & \omega L & -S_{\mathrm{D}} \\ -\omega L & -R_{\mathrm{L}} & -S_{\mathrm{Q}} \\ S_{\mathrm{D}} & S_{\mathrm{Q}} & -\dfrac{2}{3R_{\mathrm{b}}} \end{pmatrix}\begin{pmatrix} i_{\mathrm{D}} \\ i_{\mathrm{Q}} \\ V_{\mathrm{dc}} \end{pmatrix}+\begin{pmatrix} V_{\mathrm{gd}} \\ V_{\mathrm{gq}} \\ \dfrac{2\mathrm{E_g}}{3\mathrm{R_b}} \end{pmatrix}=0 \tag{33}$$

$$\begin{cases} -i_{\mathrm{sc}}^*=\dfrac{-r_2i_{\mathrm{sc}}-\sqrt{(r_2i_{\mathrm{sc}})^2+4r_2U_{\mathrm{dc}}^*[i_{\mathrm{dc}}+r_1(U_{\mathrm{dc}}-U_{\mathrm{dc}}^*)]}}{2r_2} \\ m=\frac{r_2i_{\mathrm{sc}}+r_2k_2}{-U_{\mathrm{dc}}^*}=\dfrac{-r_2i_{\mathrm{sc}}+\sqrt{(r_2i_{\mathrm{sc}})^2+4r_2U_{\mathrm{dc}}^*[i_{\mathrm{dc}}+r_1(U_{\mathrm{dc}}-U_{\mathrm{dc}}^*)]}}{2U_{\mathrm{dc}}^*} \end{cases} \tag{30}$$

The equilibrium points of the switching functions can be calculated as

$$\begin{cases} S_{\mathrm{D}}^{*} = \dfrac{-R_{\mathrm{L}} i_{\mathrm{D}}^{*} + \omega L i_{\mathrm{Q}}^{*} + V_{\mathrm{gd}}}{V_{\mathrm{dc}}^{*}} \\ S_{\mathrm{Q}}^{*} = \dfrac{-R_{\mathrm{L}} i_{\mathrm{Q}}^{*} - \omega L i_{\mathrm{D}}^{*} + V_{\mathrm{gq}}}{V_{\mathrm{dc}}^{*}} \end{cases} \tag{34}$$

We construct the matrices $\boldsymbol{J}_{\alpha}$ and $\boldsymbol{R}_{\alpha}$ as follows:

$$\boldsymbol{J}_{\alpha} = \begin{pmatrix} 0 & 0 & A_1 \\ 0 & 0 & A_2 \\ -A_1 & -A_2 & 0 \end{pmatrix}, \quad \boldsymbol{R}_{\alpha} = \mathrm{diag}\{R_3, R_4, R_5\}$$

where R_3, R_4 and R_5 are positive numbers used to vary the damping of the system.

By solving the energy matching equation (18), the control law of the VSC of the BESS can be solved as

$$\begin{cases} S_{\mathrm{D}} = S_{\mathrm{D}}^{*} - \dfrac{A_1 \left(V_{\mathrm{dc}} - V_{\mathrm{dc}}^{*}\right) - R_3 \left(i_{\mathrm{Q}} - i_{\mathrm{Q}}^{*}\right)}{V_{\mathrm{dc}}^{*}} \\ S_{\mathrm{Q}} = S_{\mathrm{Q}}^{*} - \dfrac{A_2 \left(V_{\mathrm{dc}} - V_{\mathrm{dc}}^{*}\right) - R_4 \left(i_{\mathrm{D}} - i_{\mathrm{D}}^{*}\right)}{V_{\mathrm{dc}}^{*}} \end{cases} \tag{35}$$

By solving the third equations of the energy matching equation, we can obtain

$$\begin{cases} A_1 = \dfrac{-R_3 i_{\mathrm{D}}^{*}}{V_{\mathrm{dc}}^{*}}, A_2 = \dfrac{-R_4 i_{\mathrm{Q}}^{*}}{V_{\mathrm{dc}}^{*}} \\ \dfrac{\left(i_{\mathrm{D}}^{*2} + i_{\mathrm{Q}}^{*2}\right) R_3}{V_{\mathrm{dc}}^{*2}} + R_5 = 0 \end{cases} \tag{36}$$

The new generated internal structure of the system $\boldsymbol{J}_{\alpha}$ can be expressed as

$$\boldsymbol{J}_{\alpha} = \begin{pmatrix} 0 & 0 & \dfrac{-R_3 i_{\mathrm{D}}^{*}}{V_{\mathrm{dc}}^{*}} \\ 0 & 0 & \dfrac{-R_4 i_{\mathrm{Q}}^{*}}{V_{\mathrm{dc}}^{*}} \\ \dfrac{R_3 i_{\mathrm{D}}^{*}}{V_{\mathrm{dc}}^{*}} & \dfrac{R_4 i_{\mathrm{Q}}^{*}}{V_{\mathrm{dc}}^{*}} & 0 \end{pmatrix} \tag{37}$$

By further analyzing the solution of the energy matching equation, we can obtain

$$\begin{cases} R_3 = R_4 = \dfrac{2V_{\mathrm{dc}}^{*2}}{3\left(i_{\mathrm{D}}^{*2} + i_{\mathrm{Q}}^{*2}\right) R_{\mathrm{b}}} \\ R_5 = \dfrac{-2}{3R_{\mathrm{b}}} \end{cases} \tag{38}$$

D. SYSTEM-LEVEL CONTROL STRATEGY

The unbalanced power ΔP is the difference between the output power of the wind farm P_{wind} and the grid-connected power P_{ref}, and it represents the fluctuating component of wind power that must be compensated for by the HESS to achieve the expected stabilizing effect. Because the SMES has a high power density and low energy density, it cannot conduct a high power exchange for a long period of time; thus, the high-frequency part of ΔP is assigned to the SMES. The BESS has a slow response speed, and the most serious problem of the battery is its limited cycle life, i.e., the battery cannot be charged and discharged frequently. Thus, the low-frequency part of ΔP is allocated to the BESS. That is, the SMES undergoes frequent and instantaneous power fluctuations, and the BESS addresses long-term variations.

The traditional methods for analyzing wind power fluctuation include inertia filters, wavelet decomposition, and EMD. Inertia filter methods have a certain delay, the filter constant is difficult to determine, and they cannot achieve good results in treating nonlinear and nonstationary signals. Wavelet decomposition requires a large amount of historical data, and it also cannot process nonlinear and non-stationary signals well. EMD can be used to decompose nonlinear and nonstationary signals adaptively and obtain a series of intrinsic mode functions (IMFs), which can be applied to characteristic time scales of the signal [41]–[43]. Therefore, the EMD is used to analyze the wind power fluctuations and the power distribution of the ESS. Since EMD is only a tool for allocating the initial power instructions in this paper, the basic principles of EMD are not described here.

The wind power fluctuations are decomposed into IMFs, and the frequencies of the IMFs are reduced in accordance with the order of decomposition.

The unbalanced power ΔP can be expressed as

$$\Delta P = IMF_1 + IMF_2 + \cdots + IMF_n + R \tag{39}$$

From the combination of the *IMFs* and R, we can obtain different types of power commands according to the reconstructed frequency characteristics, which are suitable for different types of ESSs.

The high-frequency components can be expressed as

$$y_{\mathrm{high}}(t) = \sum_{i=1}^{k} IMF_i = P_{\mathrm{SMES\_ref}} \tag{40}$$

The low-frequency components can be expressed as

$$y_{\mathrm{low}}(t) = \sum_{i=k+1}^{n} IMF\_i + R = P_{\mathrm{BESS\_ref}} \tag{41}$$

where $P_{\mathrm{SMES\_ref}}$ and $P_{\mathrm{BESS\_ref}}$ represent the initial power commands of SMES and BESS, respectively.

During the power allocation between the SMES and BESS, the SOC of the ESSs must be maintained at a relatively high state such that overcharge or over-discharge phenomena will not occur in the HESS. Here, we use the SMES as an example to express the real-time SOC of an SMES

$$\begin{cases} SOC_{\mathrm{SMES}} = SOC_{\mathrm{SMES\_initial}} + \Delta SOC_{\mathrm{SMES}} \\ \Delta SOC_{\mathrm{SMES}} = \dfrac{\Delta E_{\mathrm{SMES}}}{\text{SMES Capacity}} \times 100\% \end{cases} \tag{42}$$

where $SOC_{\mathrm{SMES\_initial}}$ is the initial SOC of the SMES; $\Delta SOC_{\mathrm{SMES}}$ is the SOC deviation of the SMES; and ΔE_{SMES} is the change in the SMES energy.

The acceptable SOC range of an SMES is 10-90%, and the acceptable SOC range of a BESS is 20-80%. To further ensure the safe operation of the HESS, we provided each ESS a 10% SOC margin when we designed the control rules.

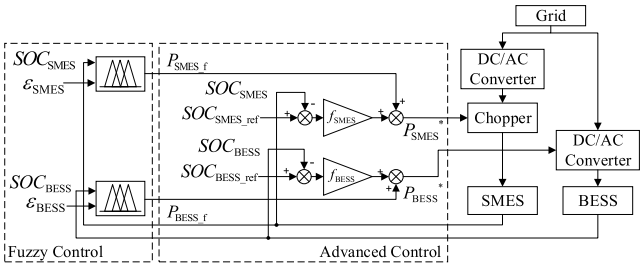

FIGURE 6. Control structure of the system-level control.

The fuzzy control and the advanced control are presented at the system level for secondary allocation of the initial power command. The fuzzy control is used to add a fuzzy logic controller for the SMES and BESS. Fuzzy logic controllers adjust the initial power commands according to the real-time SOC_{SMES}, $P_{\mathrm{SMES\_ref}}$, SOC_{BESS}, and $P_{\mathrm{BESS\_ref}}$. The advanced control is used to further adjust the power commands according to the pre-defined high-level SOC of the ESSs, which provides space for the charging or discharging to ensure that the HESS can meet the energy requirements at the follow-up time. The specific control structure of the system-level control is shown in Fig. 6, in which $P_{\mathrm{SMES\_f}}$ and $P_{\mathrm{BESS\_f}}$ represent the power commands after the fuzzy control, and P^*_{SMES} and P^*_{BESS} represent the final power commands after the complete system-level control.

The structure of the fuzzy control is shown in the left dashed box in Fig. 6. The adjustment of the power commands in the fuzzy control can be expressed as

$$\begin{cases} P_{\mathrm{SMES\_f}} = \Delta K_{\mathrm{SMES}} P_{\mathrm{sN}} + P_{\mathrm{SMES\_ref}} \\ P_{\mathrm{BESS\_f}} = \Delta K_{\mathrm{BESS}} P_{\mathrm{bN}} + P_{\mathrm{BESS\_ref}} \end{cases} \tag{43}$$

where ΔK_{SMES} and ΔK_{BESS} represent the outputs of the fuzzy logic controllers of the SMES and BESS, respectively, and P_{sN} and P_{bN} represent the rated output powers of the SMES and BESS, respectively.

After the amplitude limiting and normalization processing, the initial power instructions of the SMES and BESS can be expressed as $\varepsilon_{\mathrm{SMES}}$ and $\varepsilon_{\mathrm{BESS}}$, respectively.

The fuzzy set of $\varepsilon_x (x = \text{SMES or BESS})$ is defined as $\{NB, NS, ZO, PS, PB\}$, where NB and NS represent the deep and light discharges of the ESS, respectively; ZO indicates the power balance between the ESS and the power grid; and PS and PB represent light and deep charges, respectively. First, from the point of view of the power demand of the ESSs, the BESS undertakes the low-frequency and high-energy requirements, whereas the SMES stabilizes the high-frequency and low-energy requirements; therefore, we set the basic degree of the power flow (ZO) for the BESS within a larger range $(-0.35, 0.35)$, and a relatively tight range $(-0.25, 0.25)$ is set for the SMES. Second, from the point of view of the charge-discharge characteristics of the ESSs, the BESS has a short cycle life and is thus unsuitable for deep charging and discharging, whereas the SMES has a high power density and a long cycle life and is thus suitable

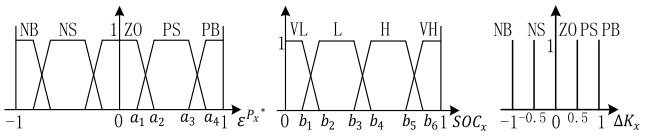

FIGURE 7. Membership functions.

for supplying high levels of power relative to its rated power. Therefore, we set the boundary for deep operation of the BESS at ± 0.65 and the boundary for deep operation of the SMES at ± 0.75. The light operation (NS, PS) of the BESS and SMES can be defined as $\mp(0.35, 0.65)$ and $\mp(0.25, 0.75)$, respectively. Thus, the parameters of the membership function of $\varepsilon^{P^*_{\mathrm{s}}}$ can be set as $a_1 = 0.125$, $a_2 = 0.375$, $a_3 = 0.625$, and $a_4 = 0.875$. Similarly, the parameters of the membership function of $\varepsilon^{P^*_{\mathrm{b}}}$ can be set as $a_1 = 0.275$, $a_2 = 0.425$, $a_3 = 0.575$, and $a_4 = 0.725$.

The fuzzy set of $\mathrm{SOC}_x (x = \text{SMESorBESS})$ can be divided as $\{VL, L, H, VH\}$, which denote 'very low', 'low', 'high' and 'very high', respectively. We divide L and H at an SOC level of 50%, and we set the extreme cases (VL and VH) based on the acceptable SOC range. Considering the security of actual operation, we provided each ESS with a 10% SOC margin. For example, the acceptable SOC range of an SMES is 10-90%; thus, the range of VL should be less than 20%, and the range of VH should be higher than 80%. Therefore, the parameters of the membership function of SOC_{SMES} should be set as $b_1 = 0.125$, $b_2 = 0.275$, $b_3 = 0.425$, $b_4 = 0.575$, $b_5 = 0.725$, and $b_6 = 0.875$. Similarly, the parameters of the membership function of SOC_{BESS} are set as $b_1 = 0.25$, $b_2 = 0.35$, $b_3 = 0.45$, $b_4 = 0.55$, $b_5 = 0.65$, and $b_6 = 0.75$.

The membership functions for the regulation factor ΔK_x (x = SMES or BESS) can be defined as $\{NB, NS, ZO, PS, PB\}$, and the domain of ΔK_x is defined as $\{-1, -0.5, 0, 0.5, 1\}$. The value of ΔK_x represents the regulation degree of power. The membership functions of the controllers are shown in Fig. 7.

It is difficult to establish a precise mathematical model for complex nonlinear control objects, and fuzzy control provides an effective way to transform expert subjective control that is based on knowledge and experience into automatic control. Determining the control rules is an important part of designing a fuzzy logic controller. However, subjective experience requires successive experiments to ensure the process's robustness and reliability, which cannot be obtained easily or rigorously. Therefore, we establish the fuzzy rules by considering the different characteristics of the ESSs and analyzing the controller's reasoning process.

The rules of the reasoning process of the fuzzy logic controller obey the following priority:

- the SOC should always be maintained in a relatively high range (H); that is, the ESSs should be able to absorb and deliver power accurately according to the commands.
- to ensure a good stabilizing effect for the following moment and reduce the pressure on the battery, we prioritize maintaining SOC_{SMES} at a relatively high state (H).

1) RULE BASE FOR THE SMES

If SOC_{SMES} is within a very high region (VH), then the fuzzy logic controller determines a different decreased value (NB orNS for ΔK_{SMES}) to modify the reference, except if the SMES needs to be discharged. Similarly, if SOC_{SMES} is within a very low region (VL), then the fuzzy logic controller must output an increased value (PB orPS for ΔK_{SMES}), unless the SMES needs to be charged.

If SOC_{SMES} is within a high range (H), $P_{\mathrm{SMES_{ref}}}$ does not need to be regulated except if there is a deep charge or deep discharge command (PB orNB for $\varepsilon_{\mathrm{SMES}}$). To ensure that SOC_{SMES} stays within a relatively high range, a minor correction (PS or NS for ΔK_{SMES}) is required when the SMES is in a deep operation.

If SOC_{SMES} is in a low region (L) (i.e., the SOC level has slightly deviated from the relatively high state), the fuzzy logic controller must output a slightly increased value (PS for ΔK_{SMES}), unless the SMES needs to be charged.

2) RULE BASE FOR THE BESS

A similar rule base to that of the SMES can be established for the BESS. Because the battery has a large capacity, SOC_{BESS} changes relatively slowly. Thus, we do not have to set a priority control when SOC_{BESS} is in a high region. If SOC_{BESS} is in a high region (H), the fuzzy logic controller outputs zero (ZO for ΔK_{BESS}); that is, $P_{\mathrm{BESS\_ref}}$ does not need any regulation.

It is also somewhat ''sensible'' to establish the same rule base for the SMES as the BESS without any priority rules. However, the analysis of the functional characteristics of ESSs shows that SOC_{BESS} changes relatively slowly because of its large capacity, while SOC_{SMES} changes by a relatively large amount and rapidly due to its low energy density. Thus, if we do not give priority to SOC_{SMES} to stay in a relatively high state (H), it would probably deviate from a good state and have an adverse effect on the stabilizing results.

TABLE 1. Fuzzy control rules.

SMES		$\varepsilon_{\mathrm{SMES}}$				
		PB	PS	ZO	NS	NB
SOC_{SMES}	VH	NB	NS	NS	ZO	ZO
	H	NS	ZO	ZO	ZO	PS
	L	ZO	ZO	PS	PS	PS
	VL	ZO	ZO	PS	PS	PB
BESS		$\varepsilon_{\mathrm{BESS}}$				
		PB	PS	ZO	NS	NB
SOC_{BESS}	VH	NB	NS	NS	ZO	ZO
	H	ZO	ZO	ZO	ZO	ZO
	L	ZO	ZO	PS	PS	PS
	VL	ZO	ZO	PS	PS	PB

The fuzzy control rules are formulated as shown in Table 1.

The structure of the advanced control is shown in the right dashed box in Fig. 6. By comparing the current SOC with a relatively high pre-defined SOC, the advanced control adjusts the power commands continuously after the fuzzy control, which optimizes the control of the SOC and reserves space for subsequent charging or discharging. Taking the SMES as an example, when SOC_{SMES} is lower than the pre-defined value $SOC_{\mathrm{SMES_{ref}}}$, the SMES is controlled to absorb more power by reducing the grid-connected power of the wind farm. In contrast, when SOC_{SMES} is higher than the pre-defined value $SOC_{\mathrm{SMES_{ref}}}$, the SMES is controlled to increase the discharging power or reduce the charging power by increasing the grid-connected power of the wind farm. The pre-defined values for the ESSs are both set to a high level (0.65) in this paper. Compared to the grid-connected power, the adjusted power for regulating the SOC in the advanced control is very small. Thus, the impact of the advanced control on the power system is almost negligible. However, the capacity of the HESS is limited, so the adjusted power can effectively maintain a good SOC level. The final power commands can be expressed as

$$\begin{cases} P^*_{\mathrm{SMES}} = f_{\mathrm{SMES}} \Delta SOC_{\mathrm{SMES}} + P_{\mathrm{SMES\_f}} \\ P^*_{\mathrm{BESS}} = f_{\mathrm{BESS}} \Delta SOC_{\mathrm{BESS}} + P_{\mathrm{BESS\_f}} \end{cases} \tag{44}$$

where $\Delta SOC_{\mathrm{SMES}}$ and $\Delta SOC_{\mathrm{BESS}}$ represent the deviations of the SOC, respectively; and f_{SMES} and f_{BESS} represent the feedback gains of the ESSs, which are determined by the capacities of the ESSs.

III. SIMULATION STUDY

The programs and simulation model were built and implemented by combining m-files and SIMULINK with MATLAB R2016a [50] and were executed on a PC with an Intel Core(TM) i7-6700K CPU (4.00 GHz) and 32 GB of RAM under Windows 10.

In order to compare the control effects of the ES control, PI control [49], model predictive control [21] and backstepping control [22], the durations of the step-change power commands are set to 1, 2 and 3 s. At 0 s, the active power command is set at 0 MW; at 1 s, it is changed to 0.5 MW; at 2 s, it is changed to 1 MW; and at 3 s, it is changed to −0.5 MW. The active power response curves of the SMES system are shown in Fig. 8. Because the BESS has similar characteristics, the waveform of the BESS is not given here. Fig. 9 shows the waveform of the magnified active power and the waveform of the reactive power.

As shown in Fig. 8 and Fig. 9, the results demonstrate that the proposed ES control strategy can effectively reduce the overshoot and setting time and can produce good power tracking results. After comparing the details, ES control achieves better control results compared to other advanced control algorithms. Among them, MP control, which does not require linear controllers and modulators, achieves adequate control results. However, MP control still requires further progress. The robustness of backstepping control is relatively poor, and it requires many computations. In addition, the waveform of the reactive power reveals that these control strategies all achieve good decoupling effects.

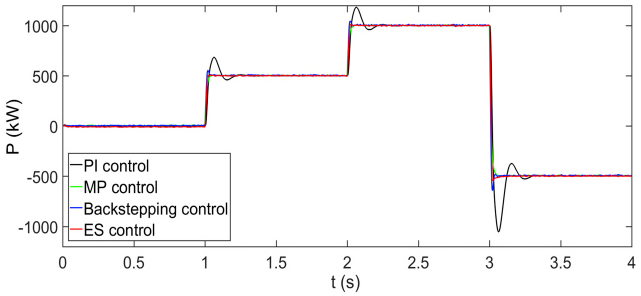

FIGURE 8. The response of the SMES under the step-change order.

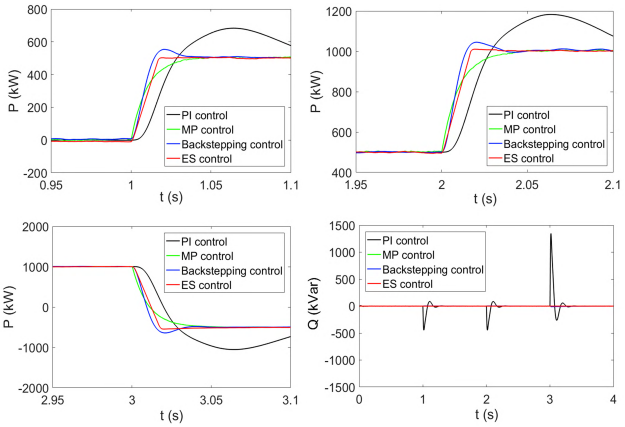

FIGURE 9. Comparison of the SMES output power.

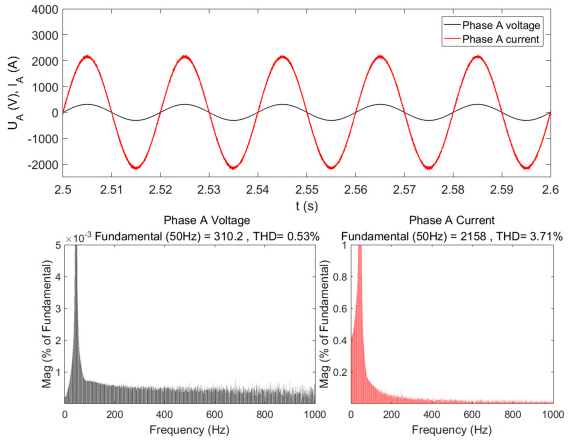

FIGURE 10. Analysis of the waveforms based on PI control.

Fig. 10 and Fig. 11, respectively, show the waveforms of the voltage and current of phase A and the corresponding spectrum analysis based on PI control and ES control.

The total harmonic distortion (THD) of the AC-side voltage is less than 0.15%, and the THD of the AC-side current is less than 1% based on the proposed ES control of the SMES system during operation. Compared to the traditional SMES system based on PI control, this result represents a considerable reduction. The output characteristic of the HESS is effectively improved by adopting the proposed ES control for the HESS.

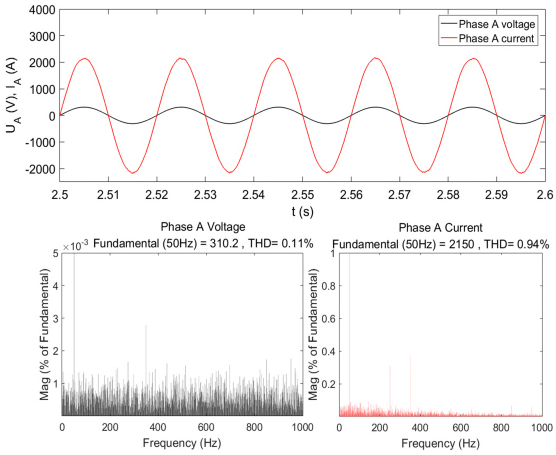

FIGURE 11. Analysis of the waveforms based on ES control.

TABLE 2. Some parameters of the model.

Wind power	mean	2.28 MW
	standard deviation	0.16 MW
SMES	rated capacity	1.8 MJ
	rated power	0.08 MW
	inductance	10 H
	running current	100 A-800 A
	DC-side voltage	800 V
	SOC limits	10%-90%
BESS	rated capacity	0.02 MWh
	rated power	0.2 MW
	rated voltage	800 V
	SOC limits	20%-80%

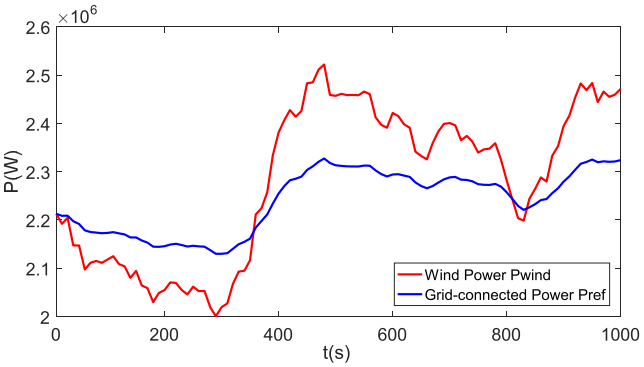

FIGURE 12. Wind power P_{wind} and grid-connected power P_{ref}.

Some of the parameters of the model are shown in Table 2.

The measured 1000 s of wind power data P_{wind} of a small wind farm and the grid-connected power P_{ref} are presented in Fig. 12.

The IMFs of ΔP are shown in Fig. 13. First, we set the upper limit of the high frequency of the battery to 0.1 Hz. IMF_3, IMF_4 and R are found to be suitable for the BESS, and IMF_1 and IMF_2 are suitable for the SMES.

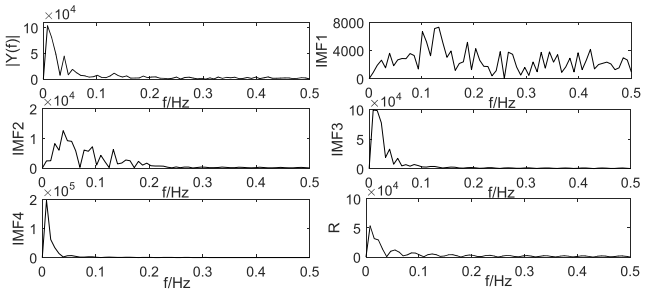

FIGURE 13. IMF components of the unbalanced power ΔP.

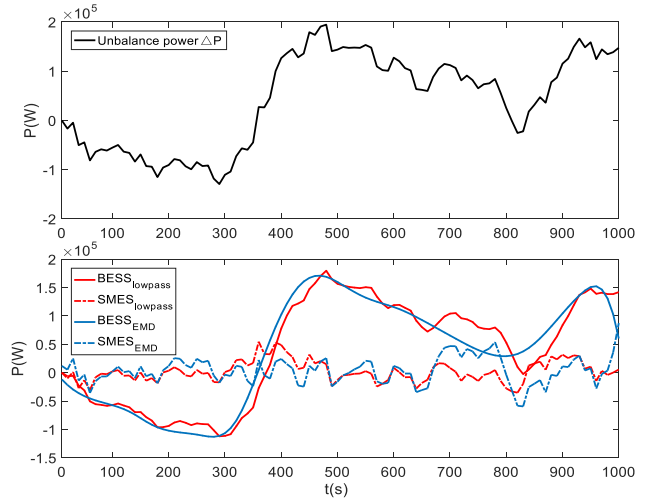

FIGURE 14. Unbalanced power ΔP and initial assigned power of the ESSs.

Fig. 14 shows the waveform of ΔP and the initial assigned power of the ESSs, which compares the performance of EMD with the low-pass filter.

For the inertial filter method, the power commands of the BESS are not very smooth, and a few burrs exist. In particular, compared with the EMD, the inertial filter method results in an obvious time lag that influences the effect of the power compensation. For the EMD method, the extent of smoothing is greater than that of the filter, and the rate of change of the battery power within a short time is reduced, achieving a certain extent of buffering. Most importantly, the EMD can overcome the delay of the response in the inertial filter method, and it also provides a considerable method to take advantage of the complementary nature of the different characteristics of the SMES system and BESS.

The adjusted power of SMES generated by the advance control at the system level can be expressed as

$$\begin{aligned} P_{\mathrm{SMES_{ad}}} &= f_{\mathrm{SMES}} \Delta SOC_{\mathrm{SMES}} \\ &= f_{\mathrm{SMES}} \left(SOC_{\mathrm{SMES_{ref}}} - SOC_{\mathrm{SMES}} \right) \end{aligned} \tag{45}$$

where $f_{\mathrm{SMES}} = \mathrm{P_{SMES\_max}} \times m$, $\mathrm{P_{SMES\_max}}$ is the theoretical maximum power absorbed by the SMES, and m is a scaling factor for the SMES.

Because the amplitude limiting method is used, the inequalities about the power commands of the SMES at the system level can be written as

$$\begin{cases} -P_{\mathrm{sN}} \le P_{\mathrm{SMES\_ref}} \le P_{\mathrm{sN}} \\ -P_{\mathrm{sN}} \le P^{*}_{\mathrm{SMES}} = P_{\mathrm{SMES\_f}} + P_{\mathrm{SMES\_ad}} \le P_{\mathrm{sN}} \end{cases} \tag{46}$$

As we need to obtain only an approximate range for m, it can be considered that $P_{\mathrm{SMES\_ref}} = P_{\mathrm{SMES\_f}}$. Then, by analyzing the data provided by the example, the inequalities about the adjusted power of the SMES $P_{\mathrm{SMES\_ad}}$ can be expressed as

$$\begin{cases} f_{\mathrm{SMES}} \left(SOC_{\mathrm{SMES_{ref}}} - SOC_{\mathrm{SMES\_min}} \right) \le 0.16 \\ f_{\mathrm{SMES}} \left(SOC_{\mathrm{SMES_{ref}}} - SOC_{\mathrm{SMES\_max}} \right) \ge -0.16 \end{cases} \tag{47}$$

where $SOC_{\mathrm{SMES\_min}}$ and $SOC_{\mathrm{SMES\_max}}$ represent the acceptable minimum and maximum SOCs for the SMES.

By calculating the above inequalities, we can get $m \le 0.5$ in this case. Therefore, we take the scaling factor m as 0.125. Similarly, the scaling factor n for the BESS is taken as 0.2. That is, $f_{\mathrm{SMES}} = 8 \times 10^4$, and $f_{\mathrm{BESS}} = 4 \times 10^4$.

A. FUZZY CONTROL RESULTS

To verify the performance of the proposed fuzzy control, two examples are chosen to illustrate the characteristics of the fuzzy rules. The curves of the input and output of the fuzzy logic controller under different conditions are plotted in Fig. 15.

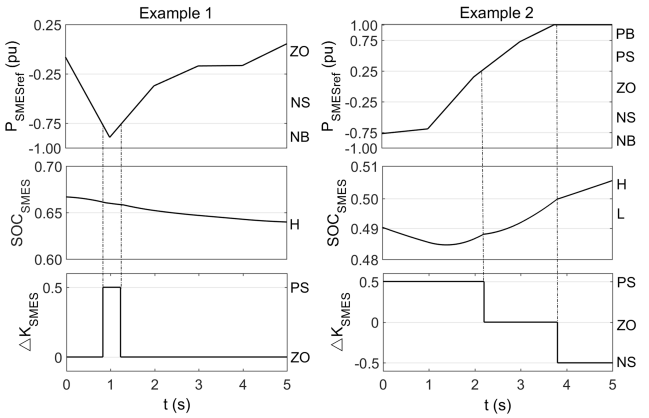

FIGURE 15. The input and output of the fuzzy logic controller in the examples.

According to the fuzzy rules set in Section II Part D, a minor correction (*NS* or *PS* for ΔK_{SMES}) is required when the SMES is in deep operation to ensure that SOC_{SMES} remains within a relatively high range (H). When SOC_{SMES} is within a low region (L), the fuzzy logic controller should output a slightly increased value (*PS* for ΔK_{SMES}), unless the SMES needs to be charged. The actual response of the fuzzy logic controller is shown in Table 3.

A comparison between the actual response in Table 3 and the expected response of the rule base in Table 1 shows that precise control is achieved by the fuzzy logic controller based on the designed rule base. Particularly, the precedence rules are triggered precisely to maintain SOC_{SMES} within a relatively high state (H).

TABLE 3. Actual response of the fuzzy logic controller.

Example 1					
$\mathcal{E}_{\mathrm{SMES}}$	ZO	NS	NB	NS	ZO
SOC_{SMES}	H	H	H	H	H
ΔK_{SMES}	ZO	ZO	PS	ZO	ZO
Example 2					
$\mathcal{E}_{\mathrm{SMES}}$	NS	ZO	PS	PB	PB
SOC_{SMES}	L	L	L	L	H
ΔK_{SMES}	PS	PS	ZO	ZO	NS

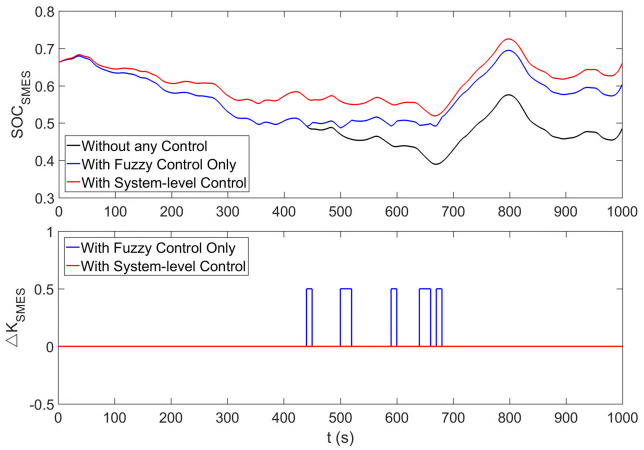

FIGURE 16. Curves of the SOC and ΔK_{SMES} of the SMES system.

B. SYSTEM-LEVEL CONTROL RESULTS

To confirm the effectiveness of the system-level control that consists of the fuzzy control and the advanced control, cases with no control, fuzzy control only, and complete system-level control are compared. The initial SOC of ESSs are set to 0.65, which indicates a good condition of ESSs.

It should be noted first that every action of the fuzzy controller will affect the power absorbed or released by the ESSs, and the actual grid-connected power will deviate from the ideal grid-connected power during this period. Therefore, under the ideal running conditions of the HESS, the SOC of the ESSs is always maintained at a relatively high state, and the fuzzy rules are not triggered during operation. When fewer rules are triggered, the actual grid-connection power becomes closer to the ideal grid-connection power; this behavior is more conducive to smoothing the grid-connected power of wind farms.

Fig. 16 shows the curves of SOC_{SMES} and ΔK_{SMES}. The results show that SOC_{SMES} remains at a low level (<50%) for a long time during the operation when no control strategy is adopted. When we use only the fuzzy logic controller to adjust the power command for the SMES, the controller adjusts ΔK_{SMES} when the fuzzy rules are being triggered. The fuzzy control can reduce the decrease of the SOC somewhat, but it cannot always maintain the SOC in a relatively high state. When the complete system-level control proposed in Section II Part D is adopted, the advanced control adjusts

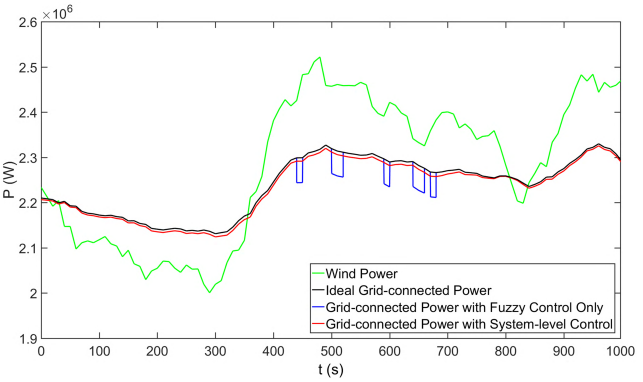

FIGURE 17. Comparison of the grid-connected power.

the power commands continuously to optimize the control of the SOC, which further improves the SOC level of the SMES and effectively prevents the SOC from triggering the fuzzy rules. Thus, the proposed system-level control has a better ability to keep the SOC within a relatively high range and reserve space for subsequent charging or discharging. Because the battery has a large capacity, SOC_{BESS} changes relatively slowly, the waveform of the SOC_{BESS} is not given here.

Since the optimized control of the SOC at the system level is achieved by reducing or increasing the grid-connected power of the wind farm, the grid-connected power with the system-level control is compared to the ideal grid-connected power with no control and the grid-connected power with only fuzzy control in Fig. 17. The adjusted power for regulating the SOC is very small compared to the grid-connected power, and the impact of the system-level control on the power system is almost negligible. Thus, the HESS with the system-level control provides an efficient grid connection for the wind farm.

IV. CONCLUSION

This paper focused on developing coordinated control strategies for a HESS based on SMES and BESS. The conclusions of this study are as follows:

1) For the HESS with nonlinear characteristics, the results reveal that the proposed ES control has better robustness than the traditional PI control and greatly reduces the difficulty of parameter tuning. Additionally, the THD of the AC-side voltage and AC-side current of the ESSs are effectively reduced, inspiring new research ideas for improving the output characteristics of HESSs and the dynamic response performance of the system.
2) EMD is used for the initial power allocation and overcomes the time lags caused by the conventional inertia filter method. Hence, EMD provides a considerable method that utilizes the different power and energy characteristics of the SMES system and BESS.
3) By considering the real-time and future SOC levels, the fuzzy control and the advanced control proposed at the system level optimize the SOC and realize the

secondary power allocation. The simulation results demonstrate that the proposed system-level control strategy can achieve reasonable power allocation and effectively optimize the SOC. The HESS can effectively smooth the grid-connected wind farm power and provide an efficient grid connection for the wind farm.

4) Future research will be conducted on the capacity allocation of the HESS, and the relationship between the economic cost of the energy storage devices and the stabilizing effect of the wind power will be analyzed. In addition, an experimental prototype of the proposed HESS will be developed in the future.

REFERENCES

[1] J. X. Jin *et al.*, "HTS power devices and systems: Principles, characteristics, performance, and efficiency," *IEEE Trans. Appl. Supercond.*, vol. 26, no. 7, Oct. 2016, Art. no. 3800526.

[2] X. Hu, S. J. Moura, N. Murgovski, B. Egardt, and D. Cao, "Integrated optimization of battery sizing, charging, and power management in plug-in hybrid electric vehicles," *IEEE Trans. Control Syst. Technol.*, vol. 24, no. 3, pp. 1036–1043, May 2016.

[3] Z. Wang, J. Hong, P. Liu, and L. Zhang, "Voltage fault diagnosis and prognosis of battery systems based on entropy and Z-score for electric vehicles," *Appl. Energy*, vol. 196, pp. 289–302, Jun. 2017.

[4] J. Wang *et al.*, "Cycle-life model for graphite-$LiFePO_4$ cells," *J. Power Sour.*, vol. 196, no. 8, pp. 3942–3948, Apr. 2011.

[5] P. Thounthong, S. Rael, and B. Davat, "Control strategy of fuel cell and supercapacitors association for a distributed generation system," *IEEE Trans. Ind. Electron.*, vol. 54, no. 6, pp. 3225–3233, Dec. 2007.

[6] L. Zhang, Z. Wang, X. Hu, F. Sun, and D. G. Dorrell, "A comparative study of equivalent circuit models of ultracapacitors for electric vehicles," *J. Power Sour.*, vol. 274, pp. 899–906, Jan. 2015.

[7] L. Zhang, X. Hu, Z. Wang, F. Sun, and D. G. Dorrell, "A review of supercapacitor modeling, estimation, and applications: A control/management perspective," *Renew. Sustain. Energy Rev.*, to be published, doi: 10.1016/j.rser.2017.05.283.

[8] L. Zhang, X. Hu, Z. Wang, F. Sun, and D. G. Dorrell, "Fractional-order modeling and State-of-Charge estimation for ultracapacitors," *J. Power Sour.*, vol. 314, pp. 28–34, May 2016.

[9] N. Sidhu, L. Patnaik, and S. S. Williamson, "Power electronic converters for ultracapacitor cell balancing and power management: A comprehensive review," in *Proc. 42nd. Annu. Conf. IEEE Ind. Electron. Soc. (IECON)*, Florence, Italy, Jun. 2016, pp. 4441–4446.

[10] S. Vazquez, S. M. Lukic, E. Galvan, L. G. Franquelo, and J. M. Carrasco, "Energy storage systems for transport and grid applications," *IEEE Trans. Ind. Electron.*, vol. 57, no. 12, pp. 3881–3895, Dec. 2010.

[11] J. Shi, Y. Liu, Y. Tang, and J. Deng, "Application of a hybrid energy storage system in the fast charging station of electric vehicles," *IET Generat. Transmiss. Distrib.*, vol. 10, no. 4, pp. 1092–1097, 2016.

[12] J. Liu, H. Zhang, and Y. Zhang, "Coordinated control strategy of scalable superconducting magnetic energy storage," *IEEE Trans. Smart Grid*, to be published, doi: 10.1109/TSG.2016.2599699.

[13] Z. Chen, X. Y. Xiao, C. S. Li, Y. Zhang, and Z. X. Zheng, "Study on unit commitment problem considering large-scale superconducting magnetic energy storage systems," *IEEE Trans. Appl. Supercond.*, vol. 26, no. 7, Oct. 2016, Art. no. 5701306.

[14] T. Moore and J. Douglas, "Energy storage, big opportunities on a smaller scale," *EPRI J.*, pp. 16–23, Spring 2006.

[15] S. Dechanupaprittha, N. Sakamoto, K. Hongesombut, M. Watanabe, Y. Mitani, and I. Ngamroo, "Design and analysis of robust SMES controller for stability enhancement of interconnected power system taking coil size into consideration," *IEEE Trans. Appl. Supercond.*, vol. 19, no. 3, pp. 2019–2022, Jun. 2009.

[16] J. Liu, H. Zhang, J. Li, B. Yang, Y. Min, and K. Yang, "A coordinated control strategy of SMES based on common DC bus," in *Proc. 40th Annu. Conf. IEEE Ind. Electron. Soc. (IECON)*, Oct. 2014, pp. 5430–5435.

[17] C. Ou and W. Lin, "Comparison between PSO and GA for parameters optimization of PID controller," in *Proc. Int. Conf. Mechatronics Autom.*, Luoyang, Henan, Jun. 2006, pp. 2471–2475.

[18] P. Liutanakul, S. Pierfederici, and F. Meibody-Tabar, "Nonlinear control techniques of a controllable rectifier/inverter-motor drive system with a small DC-link capacitor," *Energy Convers. Manag.*, vol. 49, no. 12, pp. 3541–3549, Dec. 2008.

[19] Y. Shtessel, S. Baev, and H. Biglari, "Unity power factor control in three-phase AC/DC boost converter using sliding modes," *IEEE Trans. Ind. Electron.*, vol. 55, no. 11, pp. 3874–3882, Nov. 2008.

[20] A. Allag, M. Y. Hammoudi, S. M. Mimoune, M. Y. Ayad, M. Becherif, and A. Miraoui, "Tracking control via adaptive backstepping approach for a three phase PWM AC-DC converter," in *Proc. IEEE Int. Symp. Ind. Electron.*, Vigo, Spain, Jun. 2007, pp. 371–376.

[21] T. T. Nguyen, H. J. Yoo, and H. M. Kim, "Applying model predictive control to SMES system in microgrids for eddy current losses reduction," *IEEE Trans. Appl. Supercond.*, vol. 26, no. 4, pp. 1–5, Jun. 2016.

[22] Y. Wan and J. Zhao, "Extended backstepping method for single-machine infinite-bus power systems with SMES," *IEEE Trans. Contr. Syst. Technol.*, vol. 21, no. 3, pp. 915–923, May 2013.

[23] J. Wang and H. Yin, "Passivity based controller design based on EL and PCHD model," *Proc. Eng.*, vol. 15, pp. 33–37, Jan. 2011.

[24] R. Ortega, A. J. Van der Schaft, I. Mareels, and B. Maschke, "Putting energy back in control," *IEEE Control Syst. Mag*, vol. 21, no. 2, pp. 18–33, Apr. 2001.

[25] R. Ortega and E. Garcia-Canseco, "Interconnection and damping assignment passivity-based control: A survey," *Eur. J. Control*, vol. 10, no. 5, pp. 432–450, 2004.

[26] D. Jeltsema, R. Ortega, and J. M. A. Scherpen, "An energy-balancing perspective of interconnection and damping assignment control of nonlinear systems," *Automatica*, vol. 40, no. 9, pp. 1643–1646, Sep. 2004.

[27] R. Ortega, A. V. D. Schaft, F. Castanos, and A. Astolfi, "Control by interconnection and standard passivity-based control of port-hamiltonian systems," *IEEE Trans. Autom. Control*, vol. 53, no. 11, pp. 2527–2542, Dec. 2008.

[28] R. Kelly and V. Santibanez, "Global regulation of elastic joint robots based on energy shaping," *IEEE Trans. Autom. Control*, vol. 43, no. 10, pp. 1451–1456, Oct. 1998.

[29] F. M. Serra, C. H. de Angelo, and D. G. Forchetti, "Interconnection and damping assignment control of a three-phase front end converter," *Int. J. Electr. Power Energ. Syst.*, vol. 60, pp. 317–324, Sep. 2014.

[30] H. H. Song and Y. B. Qu, "Energy-based modelling and control of wind energy conversion system with DFIG," *Int. J. Control*, vol. 84, no. 2, pp. 281–292, Mar. 2011.

[31] Y. B. Qu and H. H. Song, "Energy-based coordinated control of wind energy conversion system with DFIG," *Int. J. Control*, vol. 84, no. 12, pp. 2035–2045, Nov. 2011.

[32] H. Song, Q. Zhang, Y. Qu, and X. Wang, "An energy-based LVRT control strategy for doubly-fed wind generator," in *Proc. UKACC 11th Int. Conf. Control (CONTROL)*, Belfast, Northern Ireland, 2016, pp. 1–6.

[33] C. D. Li, H. H. Song, and Y. B. Qu, "Strategy of energy-shaping control for microgrid energy storage system in islanding operation mode," *Electr. Power Autom. Equip.*, vol. 34, no. 10, pp. 48–55, 2014.

[34] J. V. Paatero and P. D. Lund, "Effect of energy storage on variations in wind power," *Wind Energy*, vol. 8, no. 4, pp. 421–441, 2005.

[35] W. Li and G. Joos, "A power electronic interface for a battery supercapacitor hybrid energy storage system for wind applications," in *Proc. IEEE Power Electron. Specialists Conf.*, Rhodes, Greece, Jun. 2008, pp. 1762–1768.

[36] L. Shao *et al.*, "Coordinated operation strategy of storage battery SOC and smoothing wind power fluctuation," *Electr. Power Construct.*, vol. 38, no. 1, pp. 84–88, 2017.

[37] L. Bai, F. Li, Q. Hu, H. Cui, and X. Fang, "Application of battery-supercapacitor energy storage system for smoothing wind power output: An optimal coordinated control strategy," in *Proc. IEEE Power Energy Soc. Gen. Meet. (PESGM)*, Boston, MA, USA, Jul. 2016, pp. 1–5.

[38] J. W. Shim, Y. Cho, S.-J. Kim, S. W. Min, and K. Hur, "Synergistic control of SMES and battery energy storage for enabling dispatchability of renewable energy sources," *IEEE Trans. Appl. Supercond.*, vol. 23, no. 3, p. 5701205, Jun. 2013.

[39] K. Zhang, C. Mao, J. Lu, D. Wang, X. Chen, and J. Zhang, "Optimal control of state-of-charge of superconducting magnetic energy storage for wind power system," *IET Renew. Power Generat.*, vol. 8, no. 1, pp. 58–66, Jan. 2014.

[40] T. Kim, H.-J. Moon, D.-H. Kwon, and S.-I. Moon, "A smoothing method for wind power fluctuation using hybrid energy storage," in *Proc. IEEE Power Energy Conf. Illinois (PECI)*, Champaign, IL, USA, Feb. 2015, pp. 1–6.
[41] M. T. Li, S. S. Choi, K. J. Tseng, Y. Yuan, and C. C. Sun, "Design of energy storage scheme for the smoothing and dispatch planning of large-scale wind power generation," in *Proc. 5th Int. Conf. Electr. Utility Deregulation Restruct. Power Technol. (DRPT)*, Changsha, China, Nov. 2015, pp. 2113–2119.
[42] X. Yang, C. Cao, X. Li, and T. Yang, "Control method of smoothing wind power output using battery energy storage system based on empirical mode decomposition," in *Proc. 34th Chin. Control Conf. (CCC)*, Hangzhou, China, Jul. 2015, pp. 304–308.
[43] F. J. Lin, H. C. Chiang, J. K. Chang, and Y. R. Chang, "Intelligent wind power smoothing control with BESS," *IET Renew. Power Generat.*, vol. 11, no. 2, pp. 398–407, Feb. 2017.
[44] A. M. Gee, F. V. P. Robinson, and R. W. Dunn, "Analysis of battery lifetime extension in a small-scale wind-energy system using supercapacitors," *IEEE Trans. Energy Convers.*, vol. 28, no. 1, pp. 24–33, Mar. 2013.
[45] T. Chenghong, W. Jinsong, Y. Zhihong, and J. Peng, "Coordinated optimization control strategy for hybrid energy storage system based on real-time online analysis of power spectrum," in *Proc. 2nd Int. Conf. Control. Sci. Syst. Eng. (ICCSSE)*, Singapore, 2016, pp. 102–105.
[46] M. Pang, Y. Shi, W. Wang, and X. Yuan, "A method for optimal sizing hybrid energy storage system for smoothing fluctuations of wind power," in *Proc. IEEE PES Asia–Pacific Power Energy Eng. Conf. (APPEEC)*, Singapore, Oct. 2016, pp. 2390–2393.
[47] X. Han, Y. Chen, H. Zhang, and F. Chen, "Application of hybrid energy storage technology based on wavelet packet decomposition in smoothing the fluctuations of wind power," *Proc. CSEE*, vol. 33, no. 19, pp. 8–13, 2013.
[48] Z. G. Zhang, V. W. Zhang, S. C. Chan, B. McPherson, and Y. Hu, "Time–frequency analysis of click-evoked otoacoustic emissions by means of a minimum variance spectral estimation-based method," *Hear. Res.*, vol. 243, nos. 1–2, pp. 18–27, 2008.
[49] I. Ngamroo, "Optimization of SMES-FCL for augmenting FRT performance and smoothing output power of grid-connected DFIG wind turbine," *IEEE Trans. Appl. Supercond.*, vol. 26, no. 7, pp. 1–5, Oct. 2016.
[50] The MathWorks. Accessed: Aug. 1, 2017. [Online]. Available: http://www.mathworks.com

XIAODONG LIN was born in Chengdu, in 1993. He received the B.S. degree in electrical engineering from Sichuan University, Chengdu, China, in 2016. He is currently pursuing the M.S. degree in electrical engineering with Sichuan University. His research interests include the control and optimization of hybrid energy storage systems and applied superconductivity.

YONG LEI received the B.S. and M.S. degrees in electrical engineering from Southwest Jiaotong University, Chengdu, China, in 1993, and the Ph.D. degree in machinery manufacturing and automation from Sichuan University, Chengdu, China, in 2002. Since 2006, he has been an Associate Dean of the School of Electrical Engineering and Information, Sichuan University. His research interests include modern electronic technology and low-temperature superconducting techniques.